Electronic Supplementary Material (ESI) for Journal of Materials Chemistry C.

Janus β-Te_2X (X = S, Se) Monolayers for Efficient Excitonic Solar Cells and Photocatalytic Water Splitting

Jaspreet Singh[1] and Ashok Kumar[1,*]

[1]*Department of Physics, Central University of Punjab, VPO Ghudda, Bathinda, 151401, India*

(December 09, 2022)

*Corresponding Author: ashokphy@cup.edu.in

Structural, Stability and Optoelectronic Properties of β-Te_2X (X = S, Se) Monolayers

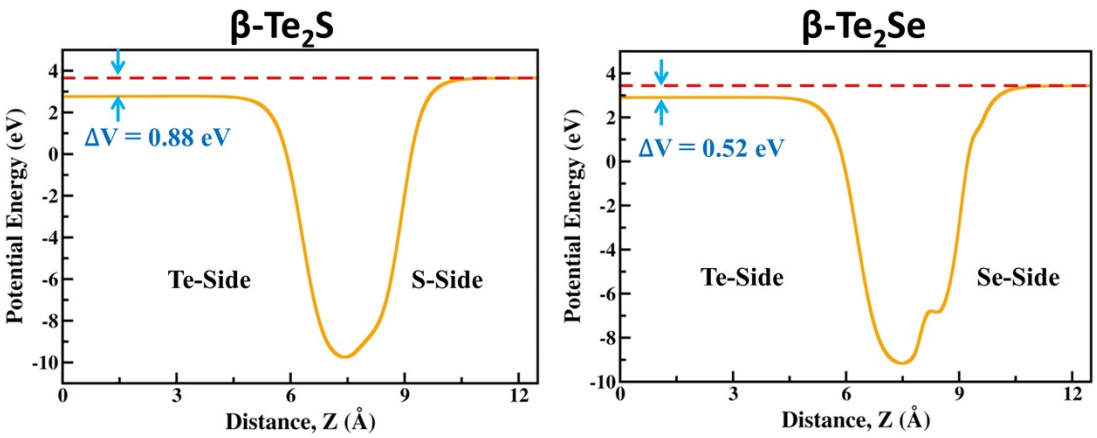

Fig. S1 The planar average of electrostatic potential energy along z-direction of β-Te_2X (X = S, Se). ΔV is the potential energy difference between two sides i.e. X and Te side.

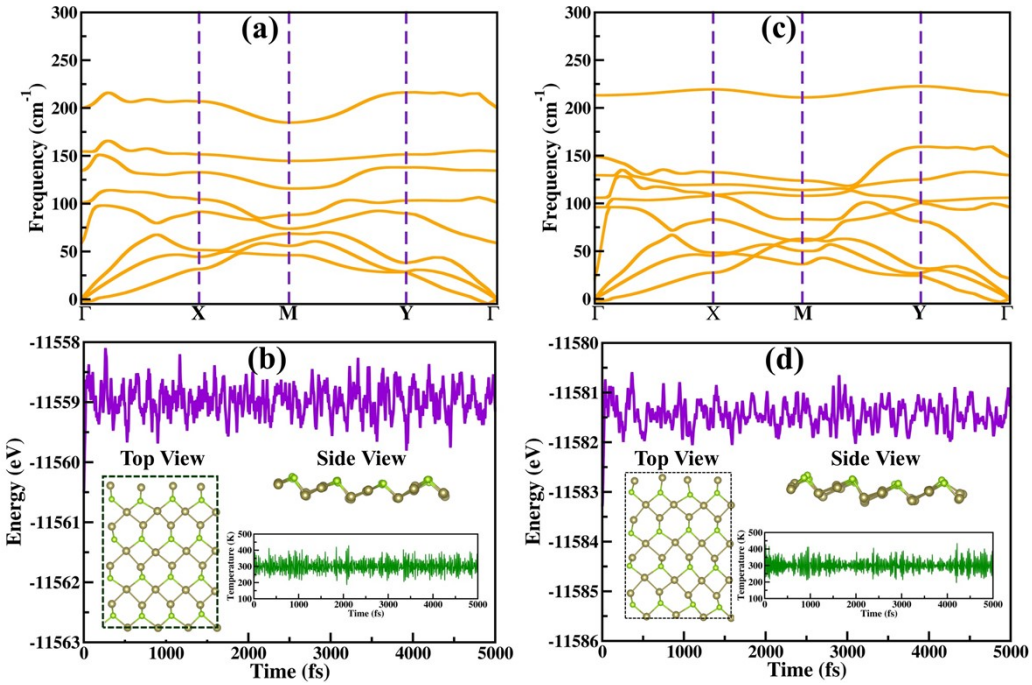

Fig. S2 Phonon and MD simulations of β-Te_2S **(a, b)** and β-Te_2Se **(c, d)**. Variation of temperature with time steps and final structures after the 5000 fs are also shown inset of **(b, d)**.

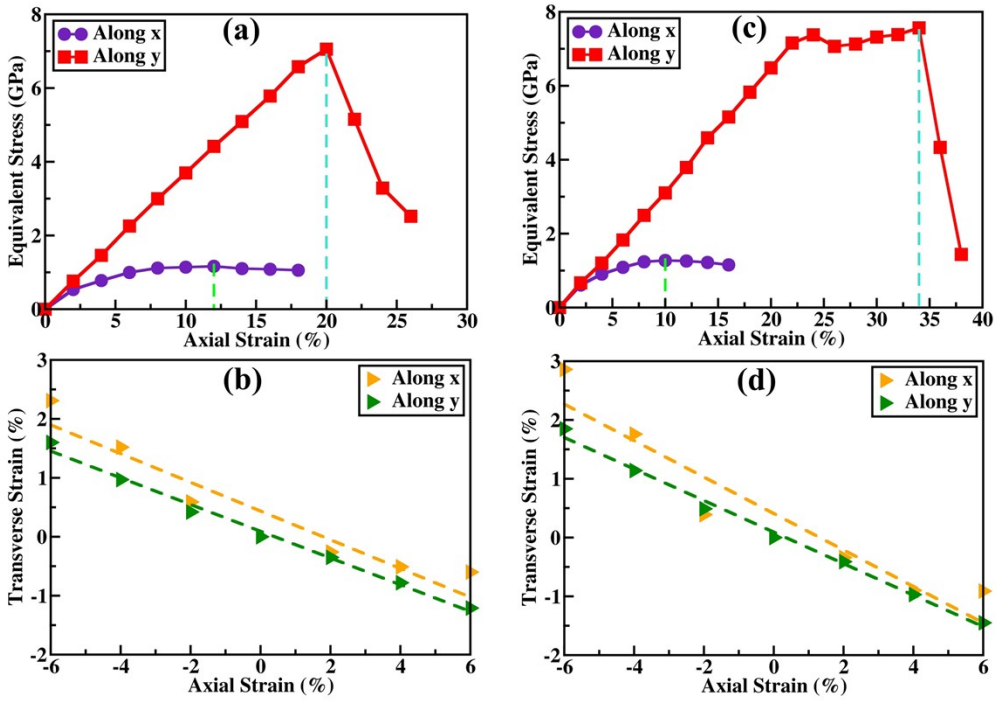

Fig. S3 Variation of equivalent stress **(a, c)** and transverse strain **(b, d)** with applied axial strain, of β-Te_2S (left panel) and β-Te_2Se (right panel), respectively.

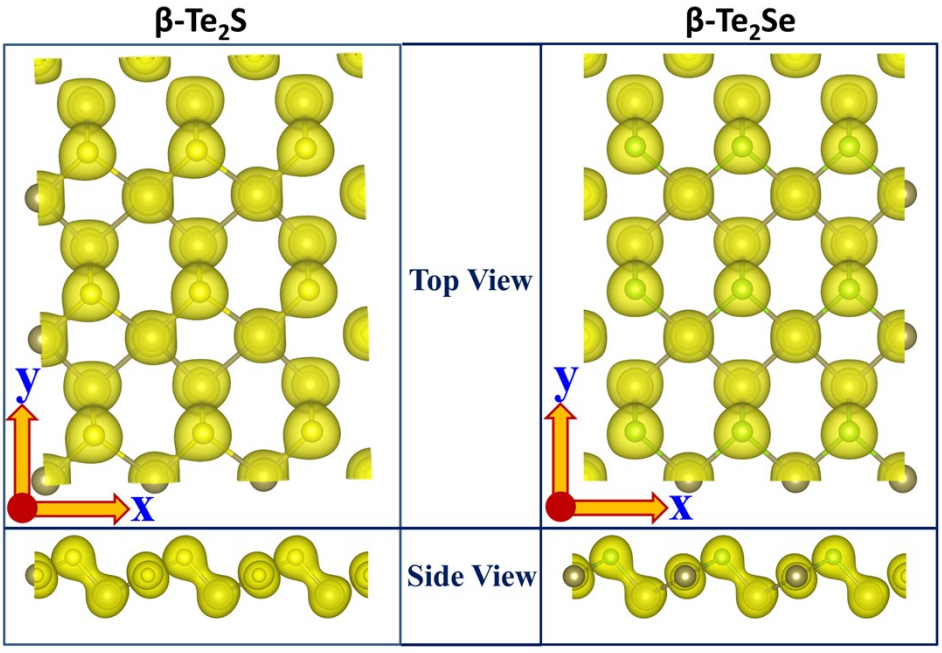

Fig. S4 The total charge density distribution of β-Te_2X (X = S, Se) monolayers. The isosurface value is 0.06 eÅ^{-3}.

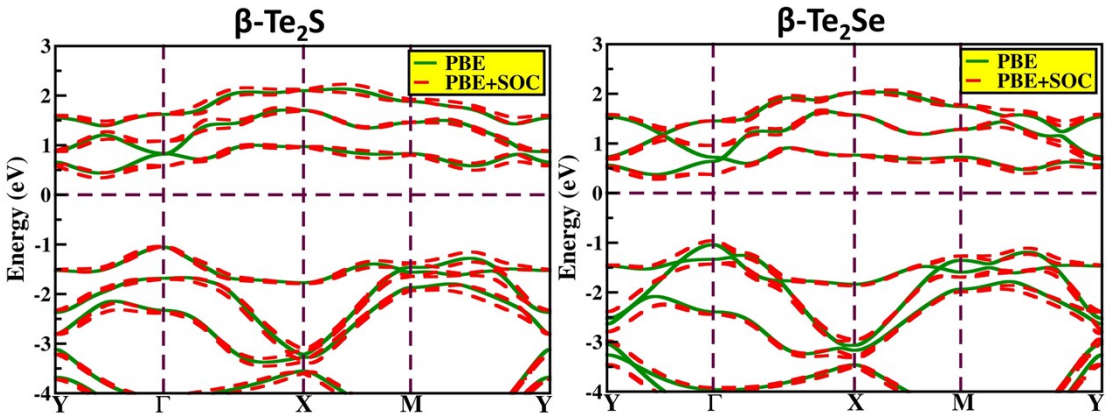

Fig. S5 Electronic band structure of β-Te_2X (X = S, Se) with PBE functional. The Fermi level is set at 0. The green and red dashed lines represent the exclusion and inclusion of SOC effect, respectively.

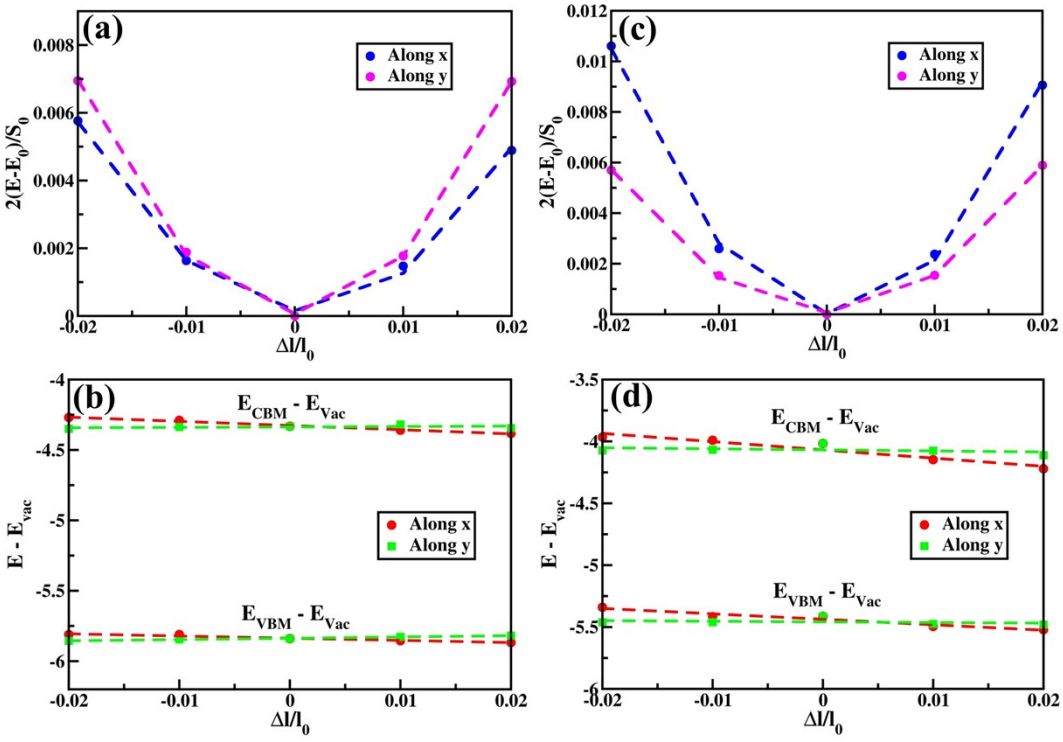

Fig. S6 Variation of $\frac{2(E - E_0)}{S_0}$ **(a, c)** and $E - E_{vac}$ **(b, d)** w.r.t strain i.e. $\frac{\Delta l}{l_0}$ with their parabolic and straight fitting, respectively of β-Te_2S (left panel) and β-Te_2Se (right panel), respectively. $E - E_0$ is the difference in the total energy of stable and strained structure, S_0 is the surface area of monolayer slab and $E - E_{vac}$ is the difference in the energy of i^{th} band and vacuum energy.

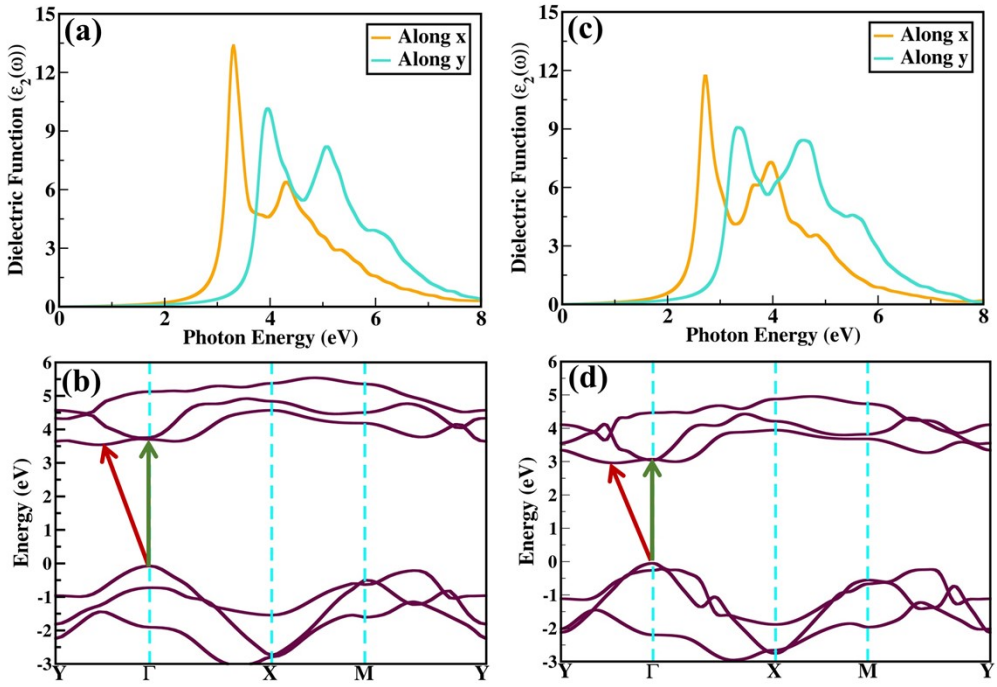

Fig. S7 Imaginary part of dielectric function ($\varepsilon_2(\omega)$) **(a, c)** and GW band Structure **(b, d)** of β-Te_2S (left panel) and β-Te_2Se (right panel), respectively. The green and red color lines in the GW band structure represent the direct and indirect quasi-particle band gaps, respectively.

Excitonic Solar Cells

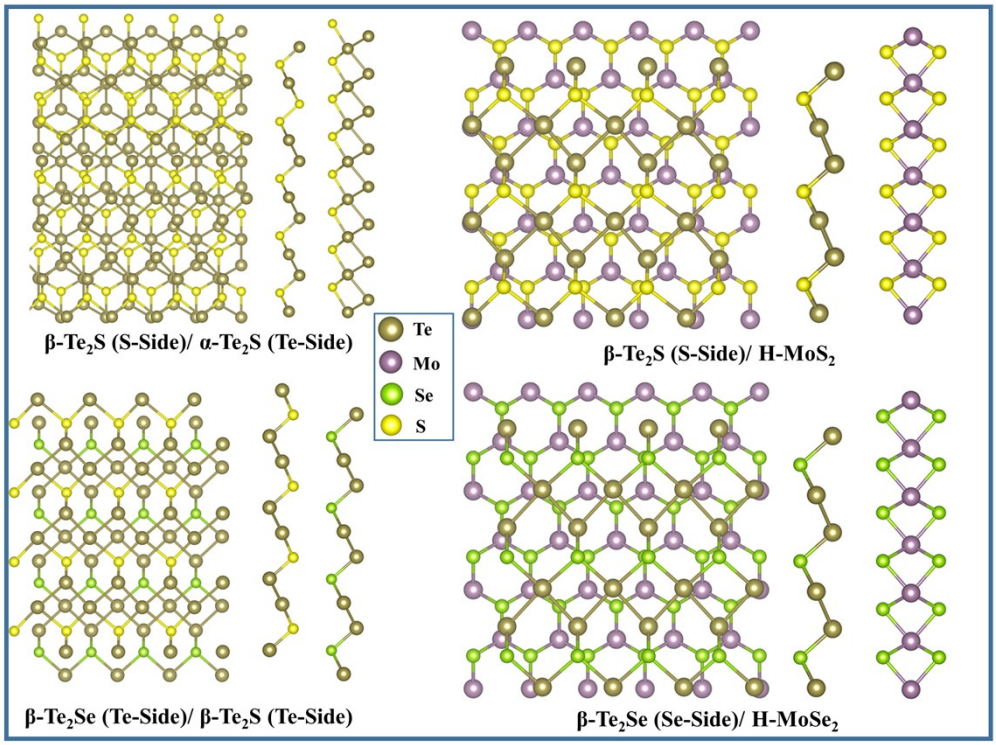

Fig. S8 Top and side views of different proposed heterostructures.

Table S1 Calculated lattice constant and band gap value with HSE method of different 2D materials taken for constructing the heterostrcutures with β-Te_2X (X = S, Se).

2D Material	Lattice Constant (Å) (Rectangular Cell) (a, b)	Band Gap (eV)
α-Te_2S	4.03, 6.98	1.49
H-MoS_2	3.18, 5.51	2.12
H-$MoSe_2$	3.32, 5.75	1.94

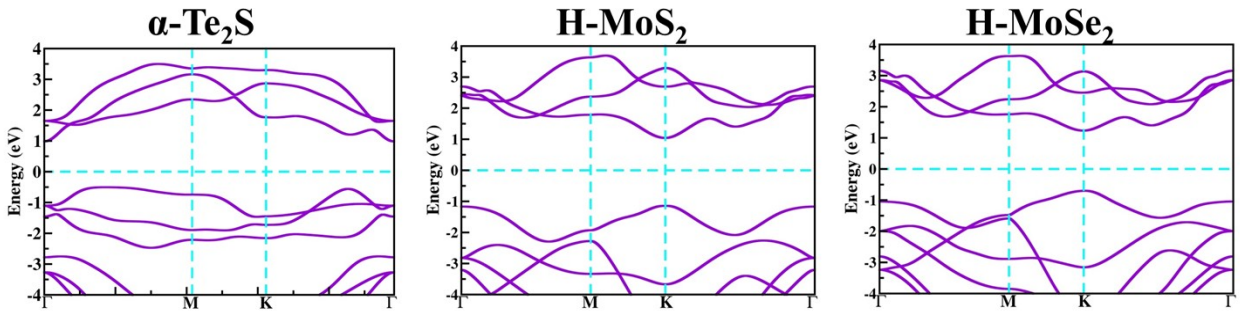

Fig. S9 Electronic band structure α-Te_2S and H-MoX_2 (X = S, Se) with HSE06 functional. The Fermi level is set at 0.

Table S2 Calculated the lattice mismatch, interlayer distance, binding energies, conduction band offsets (ΔE_c) and power conversion efficiencies (PCEs) of different proposed heterostructures for solar cells. The binding energies (E_b) per atom have been calculated using the following equation, $E_b = (E_{\text{hetero}} - E_1 - E_2)/n$, where E_{hetero}, E_1, E_2 and n, represents the total energy of heterostructure, constitutes of heterostructure and total number of atoms in the heterostructure, respectively.

Heterostructure	Lattice Mismatch (%)	Interlayer Distance (Å)	Binding Energy (meV/atom)	ΔE_c (eV)	V_{oc} (V)	PCE (%)
β-Te_2Se (Te-Side)/ β-Te_2S (Te-Side)	1.71	2.29	142.18	0.09	1.73	13.60
β-Te_2Se (Se-Side)/ H-$MoSe_2$	3.12	3.13	178.52	0.08	1.56	16.18
β-Te_2S (S-Side)/ α-Te_2S (Te-Side)	3.16	2.73	113.96	0.08	1.11	21.13
β-Te_2S (S-Side)/ H-MoS_2	3.19	3.04	159.99	0.14	1.68	13.21

Thermodynamic Oxidation and Reduction Potentials of β-Te_2X (X = S, Se) Monolayers in Aqueous Solution

Based on componential analysis and the modified approach indicated in the prior literature,[1] we believe that the photogenerated holes and electrons can reduce and oxidize the β-Te_2X monolayers by the following processes:

Reduction:

$$Te_2X + 2H_2 \rightarrow Te + H_2Te + H_2X \quad \text{(S1)}$$

Oxidation:

$$Te_2X + 2H_2O \rightarrow Te + X + TeO_2 + 2H_2 \quad \text{(S2)}$$

The thermodynamic reduction potential (ϕ^{re}) and oxidation potential (ϕ^{ox}) of β-Te_2X monolayers can be calculated as follows:

$$\phi^{re} = -[\Delta_fG^0(Te) + \Delta_fG^0(H_2Te) + \Delta_fG^0(H_2X) - \Delta_fG^0(Te_2X) - 2\Delta_fG^0(H_2)]/4eF + \phi(H^+/H_2) \quad \text{(S3)}$$

$$\phi^{ox} = [\Delta_fG^0(Te) + \Delta_fG^0(X) + \Delta_fG^0(TeO_2) + 2\Delta_fG^0(H_2) - \Delta_fG^0(Te_2X) - 2\Delta_fG^0(H_2O)]/4eF + \phi(H^+/H_2) \quad \text{(S4)}$$

The standard molar Gibbs free energy of formation (Δ_fG^0) of various products and reactants involved in reactions taken from the handbook[2] are listed in Table S3. The Δ_fG^0 of β-Te_2X monolayers are approximated by their formation energies (E_f) which is calculated as:

$$E_f = (E_{Te_2X} - 2E_{Te} - E_X)/3 \quad \text{(S5)}$$

where E_{Te_2X} is the total energy of β-Te_2X, while E_{Te} and E_X are the total energies of Te and X atoms in their stable phases. The formation energies of β-Te_2X monolayers have negligible magnitudes (~0.05 eV/atom). $\phi(H^+/H_2)$ is 0 V relative to the normal hydrogen electrode (NHE) potential, while e and F are the elementary charge and Faraday constants, respectively. After substituting these values in equations S3 and S4, the values of ϕ^{re} and ϕ^{ox} relative to NHE come out to be -0.52 V (-0.65 V) and 1.53 V (1.41 V) of β-Te_2S (β-Te_2Se) monolayers. In both the cases, the ϕ^{re} is lower than 0V, while the ϕ^{ox} is higher than 1.23 V, indication their good photoinduced corrosion resistance.

Table S3 Standard Molar Gibbs Energy of Formation ($\Delta_f G^0$) at 298.15 K in kJ/mol.

Molecular Formula	**$\Delta_f G^0$**	**Molecular Formula**	**$\Delta_f G^0$**	**Molecular Formula**	**$\Delta_f G^0$**
S	236.7	H_2S	-33.4	H_2	0
Se	187	H_2Se	15.9	TeO_2	-270.3
Te	157.1	H_2Te	84.64	H_2O	-237.1

Adsorption Energy

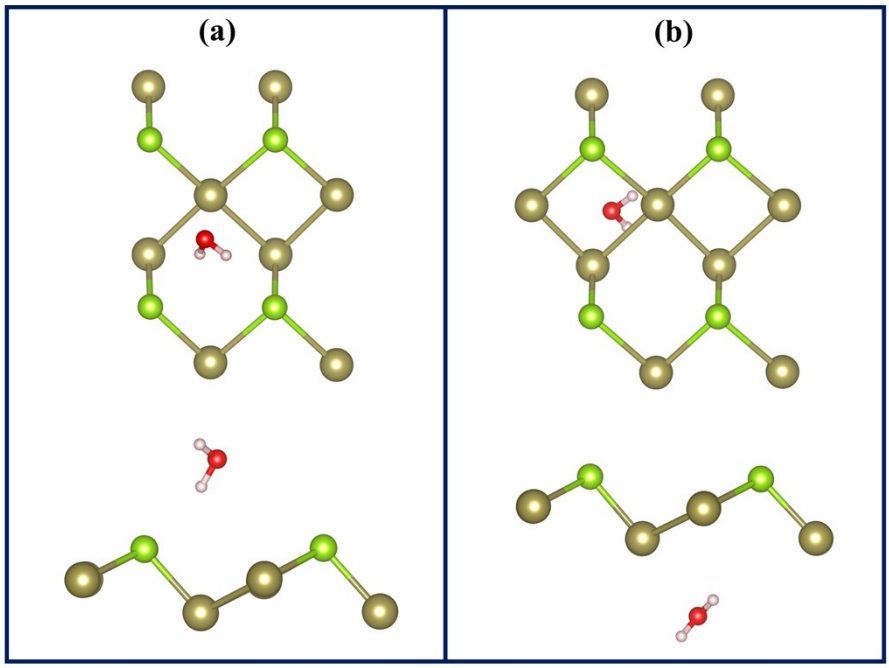

Fig. S10 Top and side views of the structures of H_2O adsorbed on **(a)** X-side and **(b)** Te-side of Janus β–Te_2X (X = S, Se) monolayer.

Gibbs Free Energy Calculations

The Gibbs free energy change (ΔG) in the water redox reactions are calculated using the hydrogen electrode model proposed by Nørskov et al.[3] as:

$$\Delta G = \Delta E + \Delta E_{ZPE} - T\Delta S + \Delta G_U + \Delta G_{pH} \quad \text{(S6)}$$

where ΔE is the adsorption energy, T is temperature (298K), ΔE_{ZPE} and ΔS are the difference in the zero point energy and entropy, respectively. ΔG_U (= $-$ eU, U is electrode potential relative to standard hydrogen electrode (SHE)) represents the extra potential of photogenerated carriers.

ΔG_{pH} (= $K_B T \times \ln 10 \times pH$) represents the contribution of Gibbs free energy at different pH concentrations. Note that the entropies of free molecules (H_2, H_2O) are taken from NIST database (https://cccbdb.nist.gov/). All these values for different species are listed in Table S4.

Table S4 Zero-pint energy correction (E_{ZPE}), entropy contribution (TS, T=298.15K), total energy (E), and the Gibbs free energy (G) of molecules and adsorbents on β-Te_2S (β-Te_2Se) monolayers. (Note: * = β-Te_2X)

Adsorbents	**E_{ZPE} (eV)**	**TS**	**E (eV)**	**G (eV)**
H_2	0.29	0.41	-31.673353371	-31.789503371
H_2O	0.58	0.58	-599.18930074	-599.19375074
*	-	-	-43057.761161412 (-49751.319001321)	-43057.761161412 (-49751.319001321)
$*O$	0.08 (0.09)	0.00	-43623.295812972 (-50316.206839647)	-43623.215012972 (-50316.118839647)
$*OH$	0.33 (0.33)	0.00	-43639.31965676 (-50332.790393409)	-43638.98555676 (-50332.460793409)
$*OOH$	0.40 (0.41)	0.00	-44203.253259282 (-50897.276554951)	-44202.856909282 (-50896.868754951)
$*H$	0.16 (0.16)	0.00	-43072.607131091 (-49766.169273406)	-43072.443831091 (-49766.007773406)

The reaction equation of two step hydrogen evolution half reaction (HER) can be written as:

$$* + H^+ + e^- \rightarrow *H \quad \text{(i)}$$

$$*H \rightarrow * + H_2 \quad \text{(ii)}$$

The free energy change for each intermediate step of HER are calculated as:

$$\Delta G_i = G(*H) - G(*) - G(H^+ + e^-) + \Delta G_U + \Delta G_{pH} \quad \text{(S7)}$$

$$\Delta G_{ii} = G(*) - G(H_2) - G(*H) + \Delta G_U + \Delta G_{pH} \quad \text{(S8)}$$

The reaction equation of four step oxygen evolution half reaction (OER) can be written as:

$$* + H_2O \rightarrow *OH + H^+ + e^- \quad \text{(iii)}$$

$$*OH \rightarrow *O + H^+ + e^- \quad \text{(iv)}$$

$$*O + H_2O \rightarrow *OOH + H^+ + e^- \quad \text{(v)}$$

$$* OOH \rightarrow * + {}^{O_2} + H^+ + e^- \quad \text{(vi)}$$

The free energy change for each intermediate step of HER are calculated as:

$$\Delta G_{iii} = G(* {}^{OH}) + G({}^{H^+ + e^-}) - G(*) - G({}^{H_2O}) + \Delta G_U - \Delta G_{pH} \quad \text{(S9)}$$

$$\Delta G_{iv} = G(* {}^{O}) + G({}^{H^+ + e^-}) - G(* {}^{OH}) + \Delta G_U - \Delta G_{pH} \quad \text{(S10)}$$

$$\Delta G_{v} = G(* {}^{OOH}) + G({}^{H^+ + e^-}) - G(* {}^{O}) - G({}^{H_2O}) + \Delta G_U - \Delta G_{pH} \quad \text{(S11)}$$

$$\Delta G_{vi} = G(*) + G({}^{H^+ + e^-}) + G({}^{O_2}) - G(* {}^{OOH}) + \Delta G_U - \Delta G_{pH} \quad \text{(S12)}$$

In these equations, the $G({}^{O_2})$ and $G({}^{H^+ + e^-})$ are calculated as; $2G({}^{H_2O}) - 2G({}^{H_2}) + 4.92$ and $1/2G({}^{H_2})$, respectively.

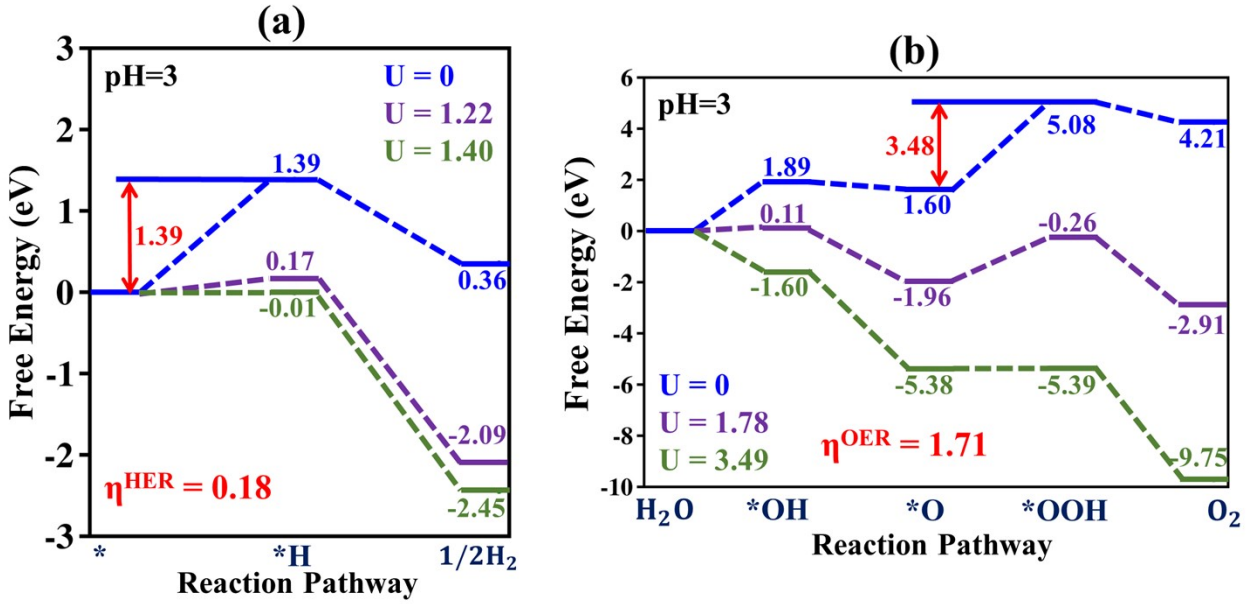

Fig. S11 The free-energy changes for **(a)** HER and **(b)** OER at pH = 3 of β–Te_2S monolayer.

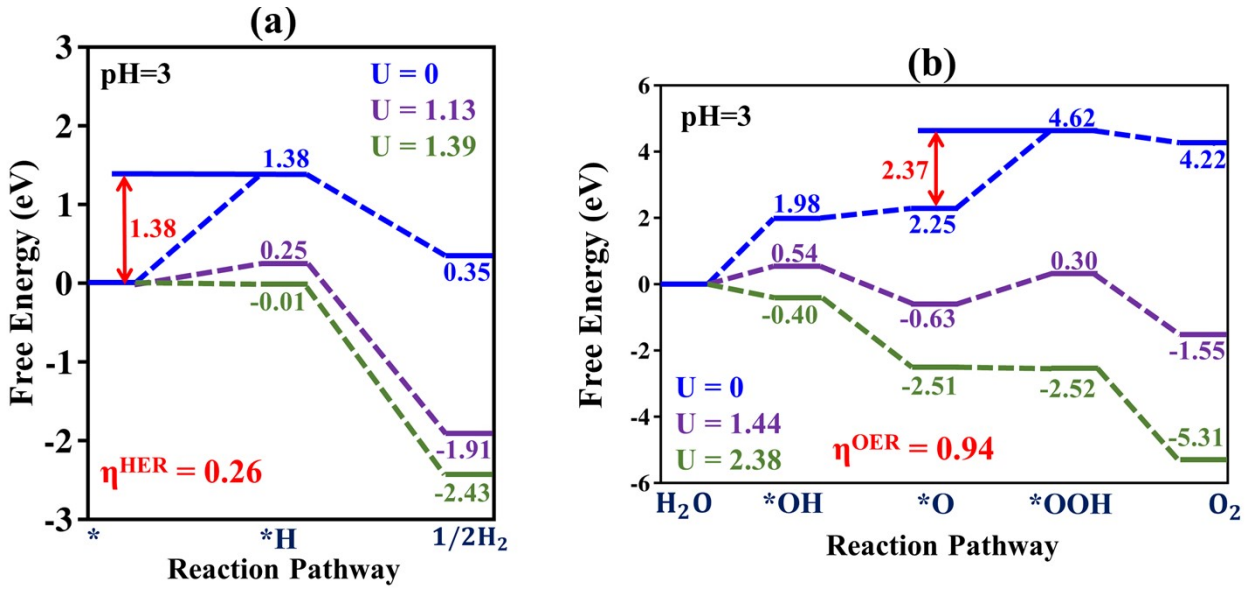

Fig. S12 The free-energy changes for **(a)** HER and **(b)** OER at pH = 3 of β–Te_2Se monolayer.

Solar-to-Hydrogen (STH) Efficiency Calculations

Table S5 Calculated Over-Potential for HER ($\chi(H_2)$) and OER ($\chi(O_2)$), energy of photons (E), energy conversion efficiency of Light Absorption (η_{abs}), Carrier Utilization (η_{cu}), Solar-to-hydrogen (STH) (η_{STH}) and corrected STH ($\eta_{STH}^{'}$) for β–Te_2S (β–Te_2Se) monolayers with the function of pH.

pH	$\chi(H_2)$ **(eV)**	$\chi(O_2)$ **(eV)**	**E (eV)**	η_{abs} **(%)**	η_{cu} **(%)**	η_{STH} **(%)**	$\eta_{STH}^{'}$ **(%)**
0	1.40 (1.31)	0.37 (0.03)	2.35 (2.62)	31.49 (34.40)	32.09 (17.17)	10.11 (5.91)	9.14 (5.52)
1	1.341 (1.251)	0.429 (0.089)	2.291 (2.561)	31.49 (34.40)	35.47 (19.60)	11.17 (6.74)	10.09 (6.30)
2	1.282 (1.192)	0.488 (0.148)	2.232 (2.502)	31.49 (34.40)	39.19 (22.18)	12.34 (7.63)	11.15 (7.13)
3	1.223 (1.133)	0.547 (0.207)	2.173 (2.443)	31.49 (34.40)	43.46 (24.87)	13.69 (8.56)	12.37 (8.00)
4	1.164 (1.074)	0.606 (0.266)	2.12 (2.384)	31.49 (34.40)	47.29 (27.54)	14.89 (9.47)	13.46 (8.85)
5	1.105	0.665	2.12	31.49	47.29	14.89	13.46

	(1.015)	(0.325)	(2.325)	(34.40)	(30.58)	(10.52)	(9.83)
6	1.046 (0.956)	0.724 (0.384)	2.12 (2.266)	31.49 (34.40)	47.29 (33.91)	14.89 (11.67)	13.46 (10.91)
7	0.987 (0.897)	0.783 (0.443)	2.12 (2.207)	31.49 (34.40)	47.29 (37.58)	14.89 (12.93)	13.46 (12.09)

The STH efficiency is defined as the product of efficiencies of light absorption (η_{abs}) and carrier utilization (η_{cu}) as proposed by Yang et al.[4] The light absorption efficiency is calculated as:

$$\eta_{abs} = \frac{\int_{E_g}^{\infty} P(\hbar\omega)d(\hbar\omega)}{\int_{0}^{\infty} P(\hbar\omega)d(\hbar\omega)} \quad \text{(S13)}$$

where $P(\hbar\omega)$ is the AM1.5G solar energy flux at energy $\hbar w$ and E_g is the band gap of material. The numerator and denominator represent the light power density absorbed by the photocatalyst and total power density of the reference sunlight spectrum (AM1.5G).

The carrier utilization efficiency is calculated as:

$$\eta_{abs} = \frac{\Delta G_{H_2O}\int_{E}^{\infty} P(\hbar\omega)d(\hbar\omega)}{\int_{E_g}^{\infty} P(\hbar\omega)d(\hbar\omega)} \quad \text{(S14)}$$

where ΔG_{H_2O} = 1.23 eV, is the water splitting potential and remaining numerator represents the effective photocurrent density. E is the actual energy of photons that utilized in water splitting, which is given by:

$$E = \begin{Bmatrix} E_g[\chi(H_2) \geq 0.2,\ \chi(O_2) \geq 0.6] \\ E_g + 0.2 - \chi(H_2)[\chi(H_2) < 0.2,\ \chi(O_2) \geq 0.6] \\ E_g + 0.6 - \chi(O_2)[\chi(H_2) \geq 0.2,\ \chi(O_2) < 0.6] \\ E_g + 0.8 - \chi(H_2) - \chi(O_2)[\chi(H_2) < 0.2,\ \chi(O_2) < 0.6] \end{Bmatrix} \quad \text{(S15)}$$

Table S6 The comparison of our calculated STH efficiencies with previously reported values for other 2D materials.

2D Materials	**STH (%)**	**Reference**
β-Te_2S, β-Te_2Se	13.46, 12.09	This work
MoSSe	15.46	[5]
In_2S_3, Al_2Se_3, Ga_2S_3	14.40, 8.00, 6.40	[4]
Penta-$PdSe_2$	12.59	[6]
WSSe	11.68	[7]
$LiInS_2$, $LiGaS_2$	9.32, 8.40	[8]
Ga_2SSe (Bilayer)	7.42	[9]
β-PtS_2, β-$PtSe_2$	2.10, 16.10	[10]

Structural and Electronic Properties of β–Te_2X Bilayers

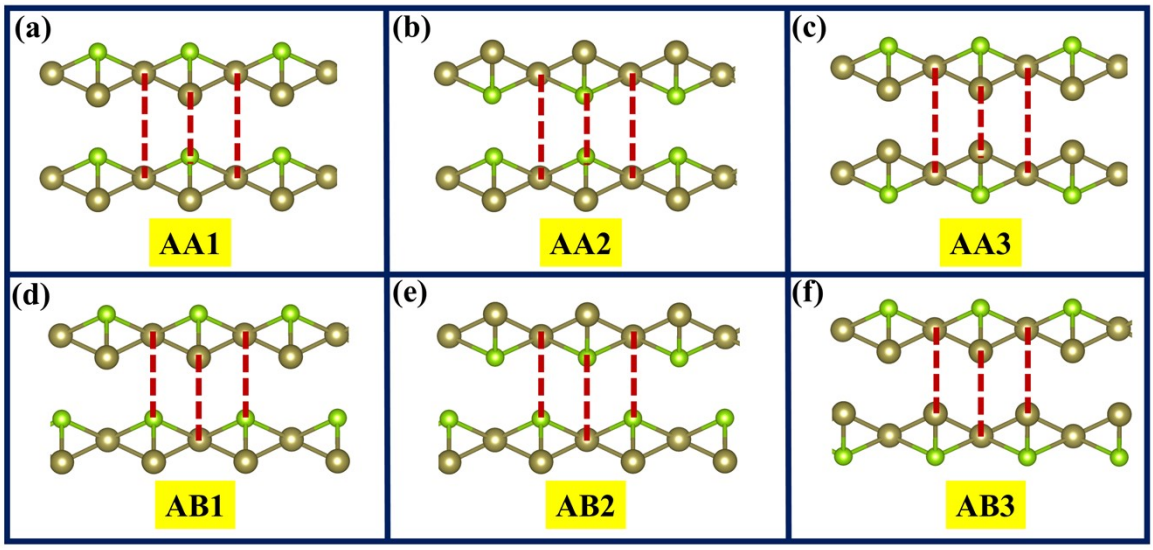

Fig. S13 Different Stacking patterns of bilayer β-Te_2X (X = S, Se).

Table S7 Calculated interlayer distance, binding energy (E_b) and potential energy difference (ΔV) for bilayer Janus β-Te_2X (X = S, Se), respectively.

Material	**Stacking**	**Interlayer Distance (Å)**	***E_b* (eV)**	ΔV (eV)
β-Te_2S	AA1	3.28	0.74	1.55
	AA2	3.07	0.72	0
	AA3	3.60	0.73	0
	AB1	2.59	0.85	1.51
	AB2	2.49	0.81	0
	AB3	2.98	0.85	0
β-Te_2Se	AA1	3.25	0.82	0.89
	AA2	3.11	0.81	0
	AA3	3.49	0.81	0
	AB1	2.22	0.99	0.83
	AB2	2.09	0.98	0
	AB3	2.50	0.97	0

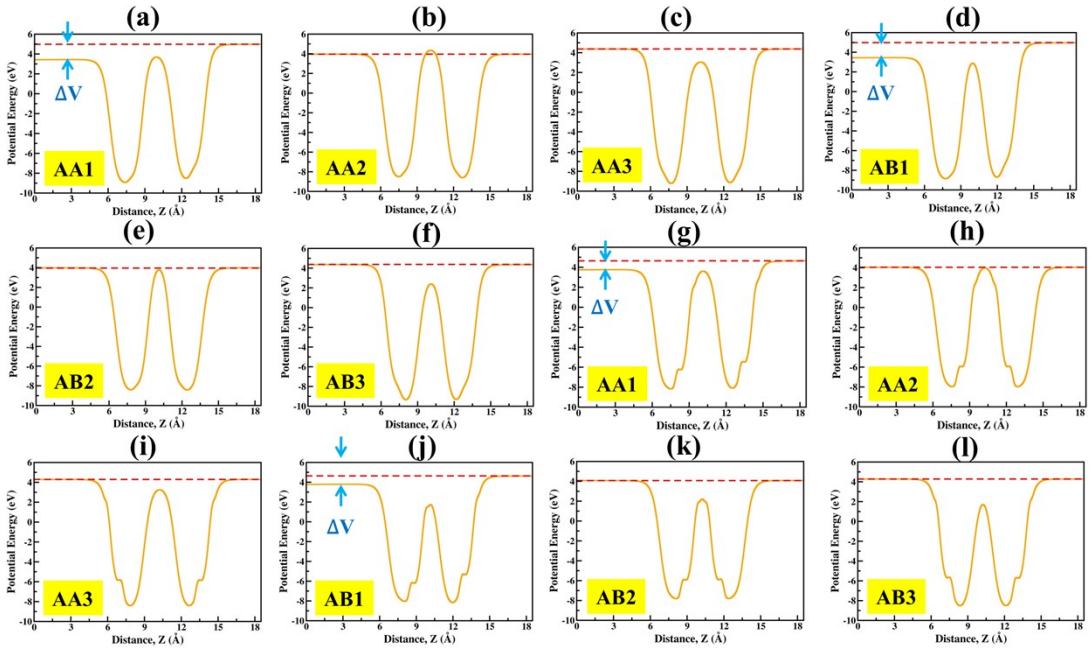

Fig. S14 The planar average of electrostatic potential energy along z-direction of differently stacked bilayers of β-Te_2S **(a-f)** and β-Te_2Se **(g-l)**.

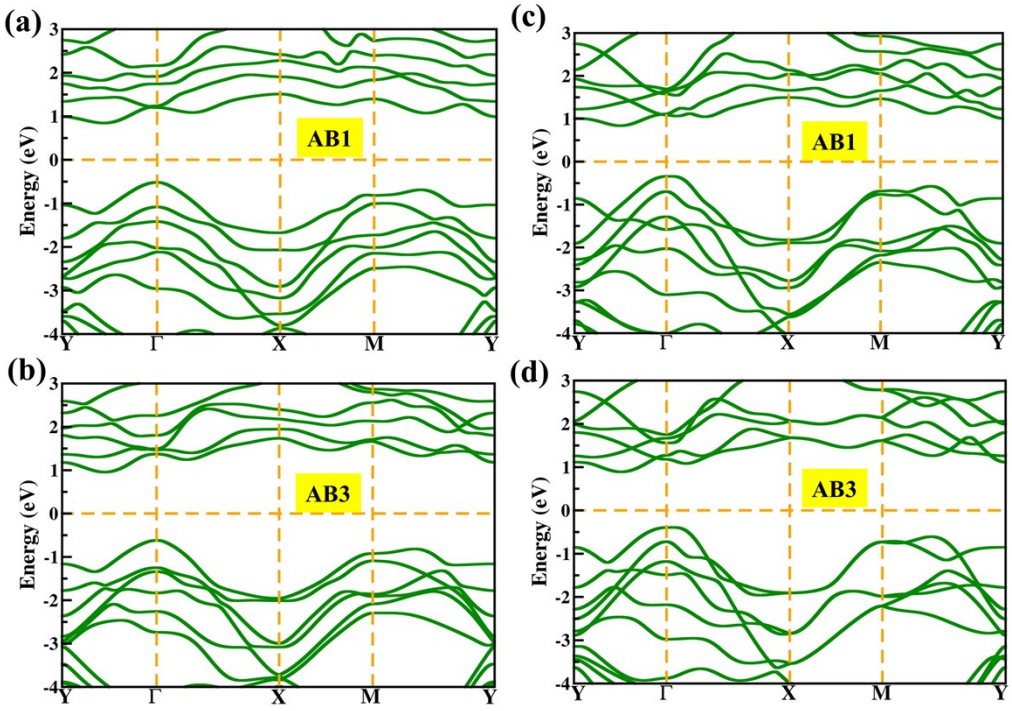

Fig. S15 Electronic band structure of bilayer β-Te_2S (a, b) and β-Te_2Se (c, d) with HSE06 functional. The Fermi level is set at 0.

References

1. S. Chen and L.-W. Wang, *Chemistry of Materials*, 2012, **24**, 3659-3666.
2. J. G. Speight, *Lange's handbook of chemistry*, McGraw-Hill Education, 2017.
3. J. K. Nørskov, J. Rossmeisl, A. Logadottir, L. Lindqvist, J. R. Kitchin, T. Bligaard and H. Jonsson, *The Journal of Physical Chemistry B*, 2004, **108**, 17886-17892.
4. C.-F. Fu, J. Sun, Q. Luo, X. Li, W. Hu and J. Yang, *Nano letters*, 2018, **18**, 6312-6317.
5. X. Ma, X. Wu, H. Wang and Y. Wang, *Journal of Materials Chemistry A*, 2018, **6**, 2295-2301.
6. C. Long, Y. Liang, H. Jin, B. Huang and Y. Dai, *ACS Applied Energy Materials*, 2018, **2**, 513-520.
7. L. Ju, M. Bie, X. Tang, J. Shang and L. Kou, *ACS Applied Materials & Interfaces*, 2020, **12**, 29335-29343.
8. Y. Fan, X. Song, S. Qi, X. Ma and M. Zhao, *Journal of Materials Chemistry A*, 2019, **7**, 26123-26130.
9. Y. Bai, R. Guan, H. Zhang, Q. Zhang and N. Xu, *Catalysis Science & Technology*, 2021, **11**, 542-555.
10. P. Jamdagni, A. Kumar, S. Srivastava, R. Pandey and K. Tankeshwar, *Physical Chemistry Chemical Physics*, 2022, **24**, 22289-22297.